Journal of Marine Research, 69, 753–777, 2011

Mean-flow and topographic control on surface eddy-mixing in the Southern Ocean

by J.B. Sallée[1], K. Speer[2] and S. R. Rintoul[3]

ABSTRACT

Surface cross-stream eddy diffusion in the Southern Ocean is estimated by monitoring dispersion of particles numerically advected with observed satellite altimetry velocity fields. To gain statistical significance and accuracy in the resolution of the jets, more than 1,5 million particles are released every 6 months over 16 years and advected for one year. Results are analyzed in a dynamic height coordinate system. Cross-stream eddy diffusion is highly inhomogenous. Diffusivity is larger on the equatorward flank of the Antarctic Circumpolar Current (ACC) along eddy stagnation bands, where eddy displacement speed approaches zero. Along such bands, diffusivities reach typical values of $3500\,m^2\,s^{-1}$. Local maxima of about $8–12.10^3\,m^2\,s^{-1}$ occur in the energetic western boundary current systems. In contrast, diffusivity is lower in the core of the Antarctic Circumpolar Current with values of $1500–3000\,m^2\,s^{-1}$, and continues to decrease south of the main ACC system. The distribution of eddy diffusion is set at three scales: at circumpolar scale, the mean flow reduces diffusion in the ACC and enhances it on the equatorward side of the current; at basin scale, diffusion is enhanced in the energetic western boundary current extension regions; at regional scale, diffusion is enhanced in the wake of large topographic obstacles. We find that the zonally average structure of eddy diffusion can be explained by theory which takes mean flow into account; however, local values depend on eddy propagation, not simply described by a single wave speed, and topography.

1. Introduction

Turbulent mixing by geostrophic eddies is an unresolved problem in large-scale ocean dynamics, and the representation of the effects of eddies in a less complex framework is desirable. Advances in representing turbulent fluxes may, for example, improve our ability to model and predict climate change. The high values of diffusion thought to occur north of the Antarctic Circumpolar Current (ACC) will strongly mix tracers in the surface layer, specifically in regions of Subantarctic Mode Water (SAMW) formation. Strong mixing will, in addition, control to some extent the propagation of freshwater and other climate signals into the ocean interior, creating local areas of large subduction (Sallée *et al.*, 2010). Although high mixing can be strongly localized, it will nevertheless have a substantial impact on the

1. British Antarctic Survey, High Cross, Madingley Road, CB3 0ET Cambridge, United Kingdom. ***email: jbsallee@gmail.com***
2. Department of Oceanography, Florida State University, Tallahassee, Florida, 32306, U.S.A.
3. CSIRO-CMAR/CAWCR/ACE-CRC, Castray Esplanade, Hobart 7000, Tasmania, Australia.

formation of SAMW. Very high values of eddy mixing associated with western boundary regions tend to spread warm subtropical water, stabilize the mixed layer, and suppress the formation of SAMW, while other high mixing regions, such as in the wake of the Kerguelen Plateau, erode the near-surface stratification, and precondition the mixed-layer for deep winter convection (Sallée *et al.*, 2006; 2008c).

Eddy kinetic energy (EKE), waves in mean flow, and bottom topography have been identified as key parameters influencing mixing intensity in the Southern Ocean (e.g. Stammer, 1998; Marshall *et al.*, 2006; Sallée *et al.*, 2008b). However, while theory has suggested links between these parameters and mixing (e.g. Holloway, 1986; Bower, 1991; LaCasce and Speer, 1999; Ferrari and Nikurashin, 2010), a consensus on the appropriate eddy mixing length and time scale has not appeared. Intense eddy activity in the surface layer of the Southern Ocean has been found to be critical in setting the strength of the near-surface branch of the meridional overturning circulation, as the circulation it induces tends to counterbalance the wind-induced transport (Sallée *et al.*, 2010), yet horizontal eddy mixing in the surface layer of the Southern Ocean is still poorly known. Despite some broad similarities, observation-based studies have proposed strikingly different views of the distribution and intensity of lateral eddy mixing (e.g. Stammer, 1998; Zhurbas and Oh, 2004; Marshall *et al.*, 2006; Sallée *et al.*, 2008b; Shuckburgh *et al.*, 2009). Estimates differ by more than one order of magnitude in some areas, and give contradictory results concerning the mixing regimes in strong jets. These discrepancies in theoretical and in observational studies continue to inhibit progress in understanding the circulation and water mass formation in the Southern Ocean.

In contrast to eddy-mixing, eddy kinetic energy (EKE) in the ocean is well known and has been widely observed with the global coverage of satellite altimetry measurements. Eddy variability at the ocean surface is structured in complex regional patterns throughout the world oceans with maxima in the western boundary currents and in the ACC of the Southern Ocean (Fig. 1b). Homogeneous turbulence theory, which describes the mixing intensity, κ, as the product of an eddy velocity u' and a mixing length scale l', has been used to derive eddy-mixing from EKE (Stammer, 1998; Keffer and Holloway, 1988). Such arguments have been supported to some extent by observations of Lagrangian trajectories. Results extracted from Lagrangian particle trajectories, analyzed either from a dispersion point of view or from Lyapunov exponent analysis, have shown that eddy-mixing may scale with EKE in western boundary current systems and in the ACC (e.g. Zhurbas and Oh, 2004; Waugh and Abraham, 2008) or with EKE above some threshold (Sallée *et al.*, 2008b).

A number of studies have, on the other hand, emphasized the importance of the mean flow in eddy-mixing, acting to reduce mixing in strong currents, such as the ACC, despite large EKE. These studies, which have arisen from the atmospheric linear wave context, predict enhanced mixing in the vicinity of steering lines, which correspond to lines where mean flow speed matches the speed of propagating meanders (e.g. Bower, 1991; Pratt *et al.*, 1995; Marshall, 2006; Smith and Marshall, 2009). In places where mean flow is large, the mean current restricts eddy length scales in the cross-stream direction, significantly

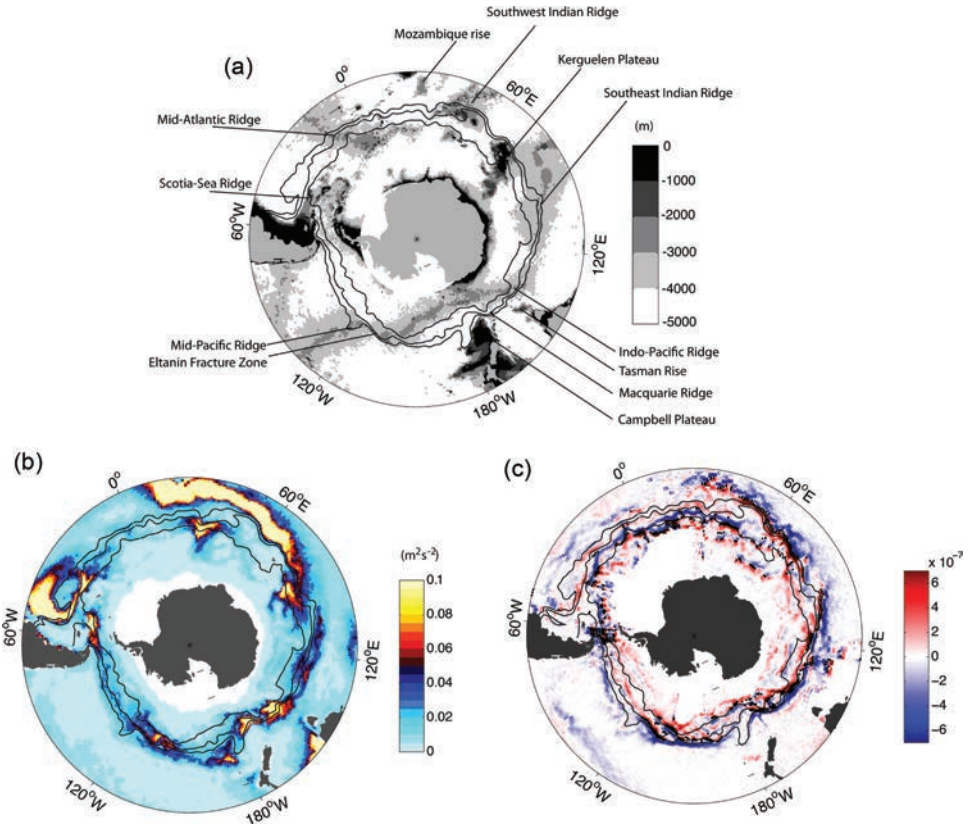

Figure 1. Dynamical characteristic of the flow — (a) Southern Ocean bottom topography. (b) Southern Ocean climatological Eddy Kinetic Energy from satellite altimetry. (c) Relative vorticity estimated from the time-mean flow. Black lines show the climatological position of three main ACC fronts (Sallée *et al.*, 2008a).

reducing the cross-stream mixing. Ferrari and Nikurashin (2010) extended this argument with a dynamical formalism allowing for weakly nonlinear perturbations, which is thought to be more realistic in an oceanic context (Chelton *et al.*, 2007). Although introducing nonlinearities changes slightly the results, the overall reduction of mixing in the core of the jets persists (Ferrari and Nikurashin, 2010).

Jets in the ACC are complicated structures that merge and emerge within a larger region of elevated eddy activity, and strong along-jet variability in cross-stream mixing might be anticipated. Witter and Chelton (1998) and Thompson (2010) have investigated numerically an idealized version of the ACC over large-scale topography showing how this complicated structure might arise and evolve, and that the associated mixing can vary enormously in time and in space. In the Southern Ocean, bottom topography (Fig. 1a) has been shown to have a large influence on the circulation and intensity of the ACC due to the topographic β-effect

(e.g. Moore *et al.*, 1999; LaCasce, 2000; Sinha and Richards, 1999; Dong *et al.*, 2006; Sallée *et al.*, 2008b). The bottom topography in the Southern Ocean has also been found to have some direct influence on mixing intensity, both on its horizontal pattern (Sallée *et al.*, 2008b; Shuckburgh *et al.*, 2009) and on its vertical structure (Lu and Speer, 2010). The mechanisms linking eddy-mixing to topography are, however, not fully understood. Topography can affect mixing by generating baroclinic-barotropic interactions (Witter and Chelton, 1998), and it can also have a large impact through the formation of a surf zone of breaking waves, in the wake of the topography (Waugh *et al.*, 1994; Rhines, 2007).

EKE, mean flow, and bottom topography, therefore, have a demonstrable influence on mixing and arguably are not independent of each other. They have, however, been given different emphasis in previous studies. Observation-based studies have principally derived Southern Ocean mixing estimates from three main approaches: tracer patch deformation (e.g. Marshall *et al.*, 2006), hydrographic variability (e.g. Joyce *et al.*, 1978; Naveira-Garabato *et al.*, 2011) and Lagrangian particle dispersion (e.g. Sallée *et al.*, 2008b). Methods allowing for a very sharp resolution of jets show a reduction of mixing in the jets (e.g. Nakamura, 1996) but hide along-stream variability that can arise from topography, and which is evident in tracer patch deformation and hydrographic variability approaches. In contrast, the standard Lagrangian particle dispersion method has difficulty with jet resolution, but shows regional variability, allowing for a description of the longitudinal structure of eddy-mixing.

Here, we use Lagrangian dispersion in stream-based coordinates to resolve both jets and regional variability to explore topographic control of near-surface mixing in the Southern Ocean. This approach allows us to demonstrate from observations that near-surface mixing in the ACC has a complex spatial structure as the result of suppression of mixing in the jets and enhancement of mixing by topographic steering and trapping of eddies.

2. Method and data

The Lagrangian particle dispersion (Taylor, 1921; Davis, 1991) method has the merit of providing spatially-dependent mixing estimates independent of any unknown coefficient. Application of this method in the Southern Ocean has consistently shown broadly enhanced mixing in the ACC, correlated roughly with EKE in higher EKE regimes (Zhurbas and Oh, 2004; Rupolo, 2007; Sallée *et al.*, 2008b). Within the ACC, longitudinal structure is strong as well (Sallée *et al.*; 2008b). Estimates of mixing by Lagrangian surface drifter observations have, however, suffered from two main limitations: the restricted number of observations, which limits our ability to resolve the jets, and a way to discriminate between cross- and along-stream diffusion. As our main interest is in cross-frontal eddy diffusion, it is important to separate accurately the along-stream and cross-stream components. Alternate coordinates have been used to account for and distinguish anisotropy due to PV conservation, mean flow, or bottom topography: f/H contours (LaCasce and Speer, 1999; O'Dwyer *et al.*, 2000); major and minor axis of the velocity covariance tensor (Sallée *et al.*, 2008b); or local mean velocity (Griesel *et al.*, 2010).

Here, diffusion is estimated from simulated trajectories based on altimetric geostrophic velocities, which allows us to work with a large number of particles to accurately resolve front scales. Sallée *et al.* (2008b) showed that geostrophic currents dominated the eddy diffusivity. We adapt the Lagrangian dispersion method to work in a longitude versus dynamic height coordinate system, which removes, to the extent that jets maintain their coherence in such coordinates, any along-stream contribution from the dispersion calculation and discriminates between mixing regimes in and out of jets (see Fig. 2). This strategy also allows us to illustrate the role of the mean flow by turning it on or off when advecting particles.

In a homogeneous flow, the absolute diffusivity is defined as the time derivative of the second central moment of particle displacement, $\overline{X^2}(t)$:

$$\kappa \equiv \frac{1}{2}\frac{d}{dt}\overline{X^2} \tag{1}$$

Under stationary conditions the diffusion coefficient can be related to the velocity autocorrelation function, and asymptotes to $\kappa_\infty = EKE\ T = EKE^{1/2}\ L$ (Taylor, 1921; Davis, 1982), where *EKE* is the eddy kinetic energy and T and L are the Lagrangian time and length scale. Previous studies have used altimetry to deduce L and T, in order to estimate the diffusivity κ. Ferrari and Nakurashin (2010) have suggested that L and T can be modulated by the presence of mean flow, so that particular care has to be taken when estimating κ from a Lagrangian length or time scale. In this study, we use the fundamental expression given in Eq. 1 rather than a length or time scale, and assume homogeneity over limited regions.

Virtual drifters are released at each 0.1 by 0.1 degree grid point in the Southern Ocean between latitude 70°S and 30°S for a total of 1,480,100 particles over the Southern Ocean. These particles are then advected using the satellite altimetry velocity field with a time-step of one day and no background diffusion. Different time steps from one hour to several days have been tested for the advection scheme, and the diffusion calculation converges when the advection time-step reaches a value of one day. We chose one day as the best compromise between the smallest error in the advection procedure and the best computing efficiency. One day is also less than the Lagrangian time scale and is, therefore, well suited to study dispersion of particles (e.g. Sallée *et al.*, 2008b).

Particles are advected for a period of one year, and the entire experiment is repeated every 6 months for the entire altimetry period, from 1993 to 2008. We perform a total of 32 ensemble particle releases, at the start of each winter (1 November) and summer season (May 1).

Dispersion time-series are computed in a 5° longitude by 1° latitude sliding window centered at grid points of a 1° longitude by 0.5° latitude grid. The choice of the scales of the sliding window is based on the typical size of an eddy loop along the trajectories, but has no particular dynamical justification. We consider these scales to be larger than the typical scale of energetic eddies but small enough to resolve substantial large-scale variability. Dispersion is computed over the 12-month trajectories of the 500 particles released in

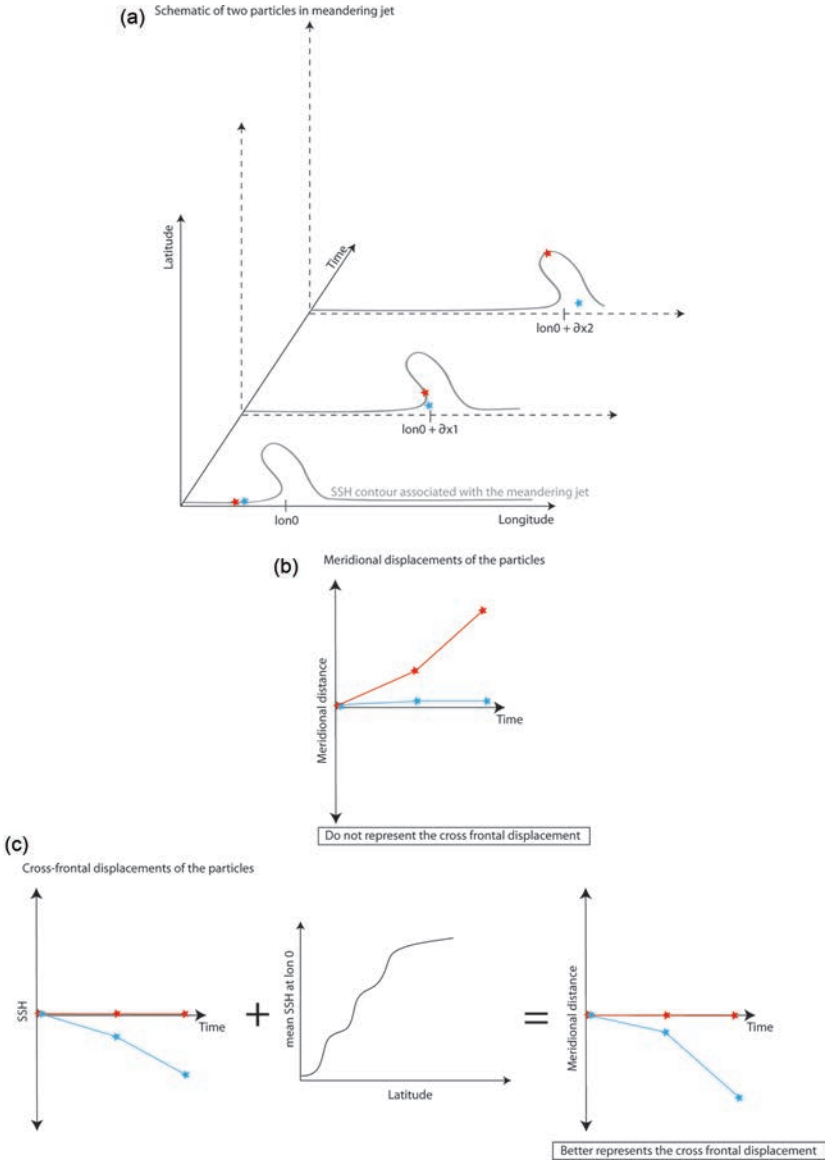

Figure 2. SSH space approach as a measure of cross-front displacement — (a) Schematic of two particles (red and blue stars) advected along a meandering jet. The SSH contour (gray line) represents the time evolving jet with a meander propagating eastward. (b) The red particle is trapped in the jet, while the blue particle crosses the jet. (b) While the red particle is advected far from its deployment position in the meridional direction, it did not cross the front; in contrast, the blue particle did not move in the meridional direction, while it did cross the front. The geographical space is therefore not adapted to detect cross-frontal displacement. (c) A plot of the instantaneous SSH at each particle position shows the cross-frontal displacement. Using the climatological mean local SSH gradient, we produce time series of "cross-frontal meridional displacement."

the sliding window (100 particles per degree bins). The mean and standard deviation of displacement are estimated over this set of particles at each time step from 0 to 360 days.

a. Velocity field

The velocity fields are deduced from the weekly maps of altimetric sea level anomaly (SLA) and altimetric absolute sea-surface height (SSH_{abs}; Rio *et al.*, 2005). The mapped SLA and SSH_{abs} fields are provided by CLS/AVISO and are based on data from the available altimeter missions (Topex/POSEIDON, ERS-1 and ERS-2, GFO, ENVISAT, JASON). The mapping technique is described by LeTraon *et al.* (1998). SLA are calculated with respect to a 7-year mean (1992-1999) and are mapped onto a $1/3°$ grid in longitude and variable grid in latitude, ranging from approximately $1/20°$ at 80°S to $1/4°$ at 30°S. A discussion of the aliased high frequency errors is given by Morrow *et al.* (2003). The altimetry data resolve wavelengths greater than 150 km, with a temporal resolution of 20 days (Ducet *et al.*, 2000). In the Southern Ocean where the groundtracks converge, the resolution improves to about 100 km. Velocity at each particle position and time are derived from this dataset using a tridimensional linear interpolation. Given the relatively coarse-resolution of altimetry dataset, a portion of the mesoscale variability might be lost and not properly resolved. However, it has been shown that for flows in chaotic advection regimes, it is the large-scale coarse-resolution velocity field that is the most important for tracer and particle advection (Haynes and Shuckburgh, 2000; Marshall *et al.*, 2006). This gives us confidence in advecting particles with the relatively coarse-resolution altimeter fields. In addition, Sallée *et al.* (2008b) showed that the cross-stream diffusive regime inferred from altimetry advected particles in the Southern Ocean is very consistent with the observed regime from *in situ* surface drifters.

b. Dynamic height coordinate system

Cross-stream displacement of a particle is reflected by a change in dynamic height (Fig. 2). Therefore, we advect particles in geographic space, and then allocated to each particle position the corresponding dynamic height To a good approximation, the cross-stream displacement of a particle is reflected by a change in dynamic height (Fig. 2). Therefore, we advect particles in geographic space, and then allocated to each particle position the corresponding dynamic height, using the instantaneous absolute sea-surface height from altimetry. The change in dynamic height along each trajectory, due to a variety of dynamical effects, is then projected back into geographical space using the local climatological sea surface height gradient (Rio *et al.*, 2005).

ACC fronts have high frequency variability in their meridional position, which can reach amplitudes of several degrees of latitude in some places (Sallée *et al.*, 2008a). Therefore, two particles at the same position, but at a different time, could be on different sides of a front. Averaging calculations over 16 years would blur the mixing regime across a front. To overcome this problem we adjust the latitudinal position of each particle using its instantaneous sea-surface height. Fronts are observed to follow contours of constant sea-surface height for large distances (Sokolov and Rintoul, 2002; 2007; 2009a,b; Sallée *et al.*, 2008a),

so that the instantaneous sea-surface height indicates the location of the particle relative to the fronts. Practically, each trajectory is allocated to the bin in which the instantaneous sea-surface height of the particle's starting point corresponds to the climatological sea-surface height.

The dispersion along each trajectory is mapped using the starting position of the particle. Therefore, the dispersion or diffusion computed at any given grid point, is representative of mixing over the area given by the typical length of particle trajectories. The typical length (standard deviation over 32 years of the bin-averaged length of the particle trajectories) spanned by particle trajectories are of order of 5–10° longitude by 1–2° latitude in energetic regions, and less in areas of weaker flow.

3. Dispersion and displacement

The central quantity in particle dispersion statistics is the Probability Density Function (PDF) of the displacement (Davis, 1991; LaCasce, 2008). As shown in Eq. 1, the diffusion is related to the time derivative of the second central moment of the displacement PDF. In this section, we present some characteristics of these fundamental quantities before tackling diffusion estimates in the next section.

a. Probability density function of particle displacement

The eddy field contains rotational components (e.g. Marshall and Shutts, 1981), leading to looping and meandering trajectories that should have no net particle dispersion (Veneziani *et al.*, 2004; 2005). Nevertheless, when particles flow through meanders or circle around eddies, oscillatory patterns are created in the dispersion time-series (Berloff and McWilliams, 2002; Veneziani *et al.*, 2004; 2005; Griesel *et al.*, 2010) that can introduce errors when computing diffusion (Griesel *et al.*, 2010). We believe that we largely overcome this difficulty by working in a dynamic height coordinate, as particles trapped in rotational motion will not significantly change their dynamic height.

In the usual Lagrangian dispersion treatment, the action of energetic rotational coherent structures introduces a departure of the displacement PDF from Gaussian (Bracco *et al.*, 2000a,b; Sallée *et al.*, 2008b). Rotational motions and front meandering will cause the kurtosis to be lower than 3, as the meridional displacement will be dominated by large and alternating southward and northward movements (Bracco *et al.*, 2000a; Hughes *et al.*, 2010). This poses a problem for the application of the Lagrangian dispersion formalism to tracer diffusion, which assumes that displacement PDFs are at least approximately Gaussian (Davis, 1991). Our dynamic height procedure reduces non-Gaussian behavior, because it naturally minimises the effect of rotational motion or meandering jets (Fig. 3).

b. Dispersion time-series

Figure 4a,b shows the dispersion calculated in the ACC sector, between the Polar Front (PF) and the northern branch of the Subantarctic Front (SAF-N) using the frontal definitions

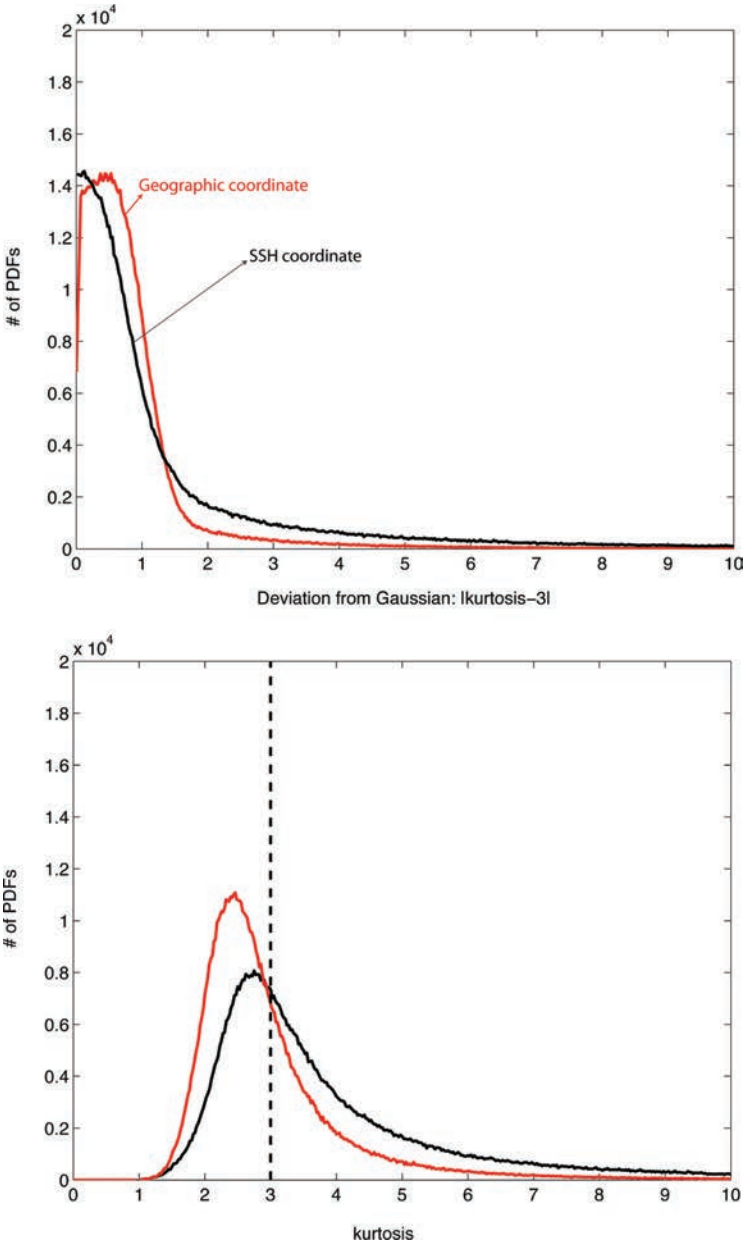

Figure 3. Statistical analysis of displacement PDF — (a) Histogram of |kurtosis-3|(i.e. the deviation from Gaussianity) from displacement PDFs, for all PDFs generated in each bin of the Southern Ocean, and for the 32 particle-releases between 1993–2008. (b) Histogram of kurtosis from displacement PDFs, for all PDFs generated in each bins of the Southern Ocean, and for the 32 particle-releases between 1993–2008.

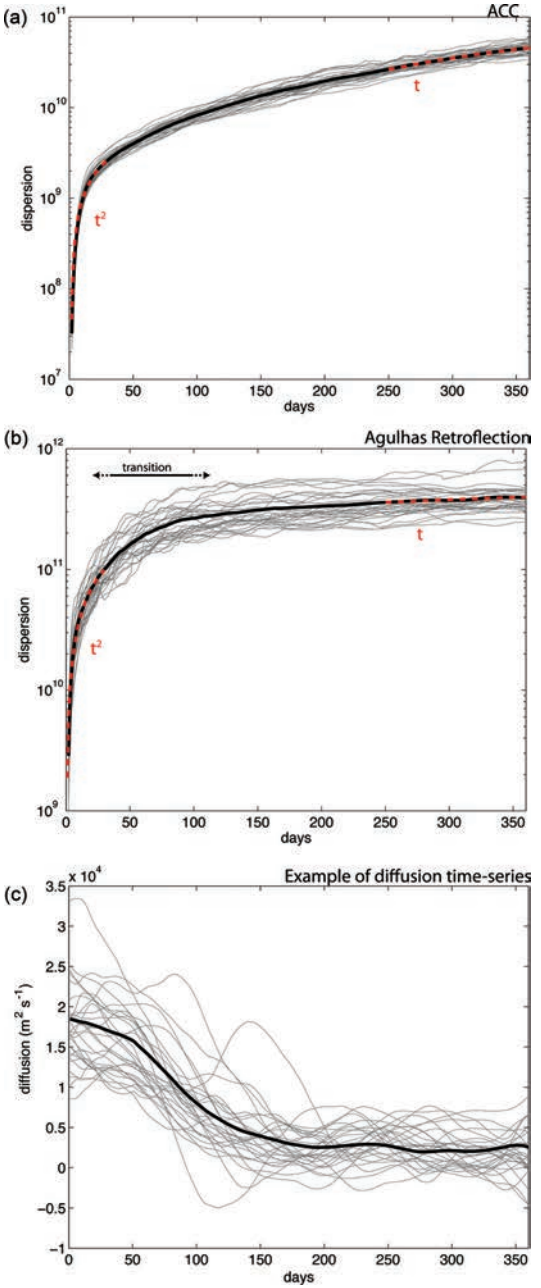

Figure 4. Averaged dispersion time series for the entire (a) ACC region and in (b) the Agulhas Retroflection region. Dispersion for each of the 6-month launch between 1992–2008 (grey) and climatological mean dispersion (black). Best polynomial fit are shown in red for the periods 0–15 days and 250–360 days. (c) Example of diffusion time-series obtained in an energetic region within the ACC in the vicinity of the southwest Indian Ridge (50°E) for each of the 6-month launch between 1992–2008 (grey) and climatological mean diffusion time-series (black). This example illustrates the large variability of diffusion coefficient at early times. In the particular case displayed, a stable diffusion is obtained around 200 days.

of Sallée *et al.* (2008a), and in the Aghulas Retroflection sector where previous studies have shown a large enhancement of EKE and mixing (Fig. 1b; Sallée *et al.*, 2008b; Waugh and Abraham, 2008). Consistent with previous studies, two regimes are detected: a transition time with periods less than approximately 50 days where dispersion grows quadratically, and a second regime where the dispersion converges towards linear growth (Taylor, 1921; LaCasce, 2008; Sallée *et al.*, 2008b). In this paper we focus on the linear regime. The linear growth regime starts at around 70–90 days. Griesel *et al.* (2010) showed from modeled float trajectories that the diffusion estimated at around 100 days is well representative of the diffusion up to 600 days, suggesting that the linear regime holds for long times. Furthermore, previous Southern Ocean studies have shown that periods between 40 h and 90 days account for most of the eddy signal (Nowlin *et al.* (1985) for observations in the Drake Passage; Phillips and Rintoul (2000) for the region south of Australia). Griesel *et al.* (2010) illustrated that diffusion can be strongly overestimated by integrating over periods that are too short. Indeed, in highly energetic areas with large rotational components the linear growth starts later. We note that this time window is associated with the time-lag at which the velocity autocorrelation reaches an asymptotic behavior. In contrast, the Lagrangian time scale is associated with the time at which the velocity decorrelates and is typically of order of a few days (e.g. Sallée *et al.*, 2008b). The two quantities do not match because of negative and positive lobes in the velocity autocorrelation at long lags (eg. Sallée *et al.*, 2008b; Griesel *et al.*, 2010). The Lagrangian time-scale (T_L) is related to the eddy-diffusion intensity and eddy spatial scale (L_{co}; see Section 5).

As shown by Griesel *et al.* (2010), the estimate is sensitive to the choice of time window. Figure 4c shows an example of diffusion time-series obtained in an energetic region within the ACC in the vicinity of the southwest Indian Ridge (50°E). This example illustrates the large variability of diffusion coefficient at early times. In the particular case displayed, a stable diffusion is obtained around 200 days. There are still some lobes after 200 days but they oscillate around a constant diffusion value. We, therefore, compute diffusion using the mean value of diffusion in the window 250–360 days. A choice of a window of 50–150 days (similar to Sallée *et al.*, 2008b) would produce a mixing coefficient roughly twice as large as that using the window 250–360 days. We make the conservative choice of focusing on the time window 250–360 days as the longest time period that still resolves regional structure in the diffusion coefficient.

c. Errors

The error on the cross-stream diffusion coefficient calculation is estimated with a Monte-Carlo experiment. The 360-day advection of each of the 1,480,100 particles is repeated fifty times for each of the 16 releases between 1993 to 2000. The Monte-Carlo experiment is only performed on the first half of the altimetry period (1993–2000) because of the large computing time involved in 50 realizations of the same experiment. For each of the 50 realizations of the calculation, we add to the altimetry field a time and space variable random error in the

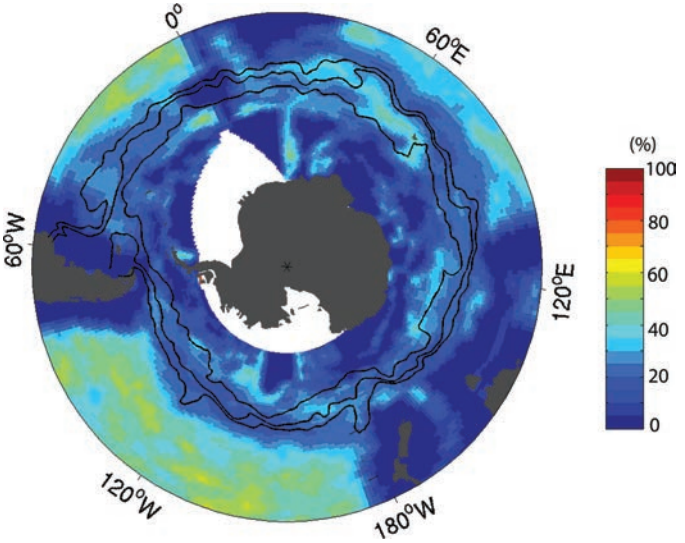

Figure 5. Error map — (a) Ratio of the resulting standard deviation of 50 Monte-Carlo experiments over mean value of diffusion for the year 1993–2000. The 8-year diffusion calculation is repeated 50 times with a random error within a range of ±5 cm added to the altimetry sea-surface height field.

range $\epsilon(x, y, t) \in [-5 + 5]$ cm. The error propagates into the calculation of the trajectory through the velocity derived from the sea-surface height, and into the cross/along-stream dispersion projection. The impact of the ±5 cm random error on the resulting diffusion is estimated for each of the 16 releases between 1993 to 2000 from the standard deviation of diffusion coefficient produced by the 50 Monte-Carlo realizations. We define the mean error of our calculation as $Error = \frac{\overline{sqrt(\sigma(\kappa_{\epsilon\in[-5+5]}))}^{1993-2000}}{\kappa_{\epsilon=0}}$, where $\sigma(\kappa_{\epsilon\in[-5+5]})$ is the variance of the 50 Monte-Carlo realizations with a random error $\epsilon(x, y, t)$, and $\overline{(.)}^{1993-2000}$ is the time average over the years 1993–2000. The error in the ACC is relatively small, of the order of 10–20% of the estimated diffusion (Fig. 5). However, the standard deviation peaks north of the ACC at 50%, in areas of weak flow. The regional pattern reflects the fact that the error is small in areas of large sea-surface height gradient and large in areas of low sea-surface height gradient. Indeed, in low SSH gradient regions, a small SSH error would produce a large departure of the particle trajectory and, therefore, large errors on the diffusion coefficient. We consider the standard deviation as an estimate of the variability of the results; standard error, in contrast, would be smaller by a factor of $\sqrt{50}$.

4. Regional variability of surface eddy diffusivity

The 16-year mean cross-stream eddy diffusivity (κ) has been computed with and without the mean flow (Fig. 6a,b). Maximum diffusion is observed in the Agulhas Retroflection

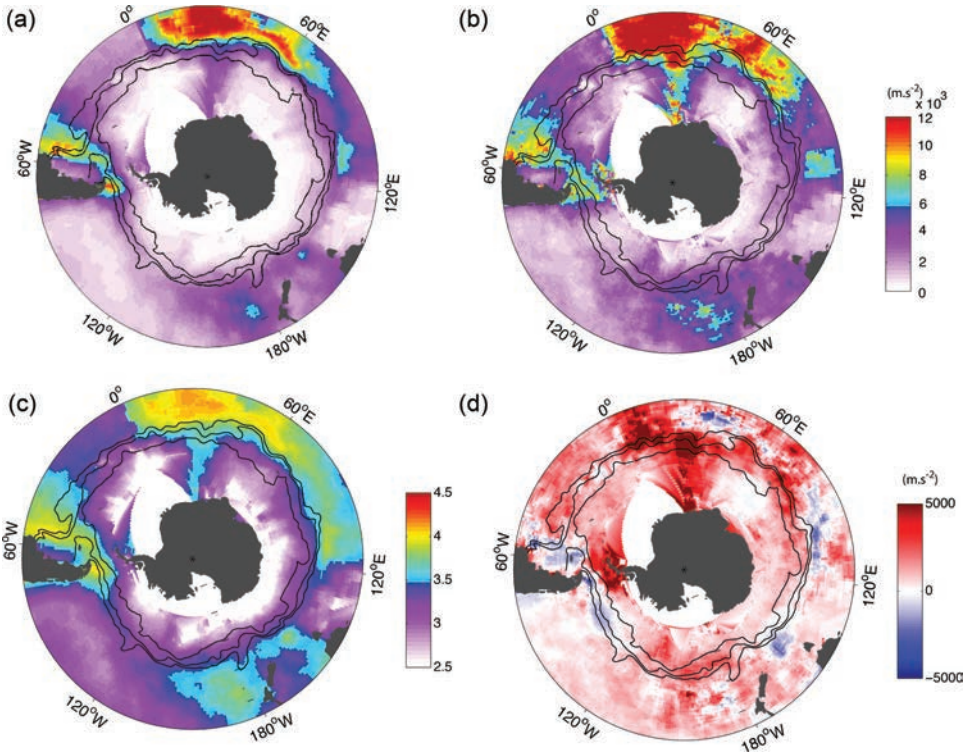

Figure 6. Diffusion in the Southern Ocean — Diffusivity when mean flow is turned (a) on or (b) off. (c) Log_{10} of the diffusivity with mean flow turned on (same as in panel a). (d) Difference between estimates without and with mean flow. Black lines show the climatological position of three main ACC fronts (Sallée *et al.*, 2008a).

between 30°E and 70°E. Dritschel and McIntyre (2008) argue that the barrier to cross-jet mixing characteristic of a jet can break down in the presence of large vortices if they are associated with PV anomalies larger than the PV step of the jet itself. The Aghulas retroflection region is certainly a place with intense eddy formation (Fig. 1b), where the barrier notion could partially break down.

Diffusion is generally high in other western boundary current regimes throughout the Southern Ocean as well, specifically across the southwestern Atlantic in the Brazil-Malvinas Current area (50°W; $\kappa \approx 6$–$10\ 10^3\ m^2\ s^{-1}$), the region east of New Zealand ($\kappa \approx 4$–$6\ 10^3\ m^2\ s^{-1}$), near 170°W, 50°S (see also Bryden and Heath, 1985; Shuckburgh *et al.*, 2009). High diffusion is also associated with major topography features such as the Macquarie Ridge region at 150°E, and the Southeastern Indian Ridge region at 110°E ($\kappa \approx 4$–$6\ 10^3\ m^2\ s^{-1}$). These regions are all subject to control by the details of the distributions of EKE, eddy stagnation (hence mean flow), and length scale, such that a simple characterization by any one field is not sufficient.

The dominance of the Agulhas Retroflection region means that care must be taken in the calculation and interpretation of zonal averages; the dynamic height coordinate makes the distinction between this region and ACC flow stronger, and helps to separate mixing effects that are otherwise merged.

Away from western boundaries, surface diffusion generally falls off. Exceptions are the long tail of high diffusion in the downstream Agulhas retroflection and weaker extensions from other western boundary current regions, an isolated maximum near 110°E, and the north-south ridges of higher diffusion in Drake Passage and along 30°E. The Drake Passage maxima are near the location where several fronts come close together and, occasionally, merge, forming a very intense jet. Along about 30°E, the Polar Front crosses the SW Indian Ridge in a narrow gap near 52°S, and experiences strong meandering downstream of the ridge. The southward extension of this high mixing may be related to variability of the eastern end of the Weddell Gyre (e.g. Fahrbach *et al.*, 1994; Shröder and Fahrbach, 1999).

Large-scale patterns of κ show some similarities with previous results investigating diffusion from Lagrangian dispersion or altimetry (e.g. Stammer, 1998; Rupolo, 2007; Zhurbas and Oh, 2004, Sallée *et al.*, 2008b; Waugh and Abraham, 2008). In general, the strongest variations in mixing were associated with strong variations in EKE, though functional relationships were neither uniform nor clearly identified across different regimes of the ACC. Here, no consistent relationship is found. In addition, we find two main differences with previous studies based on altimetry or Lagrangian dispersion: (i) diffusion is reduced within the fronts of the ACC, and (ii) peak values are significantly smaller.

The diffusion in the ACC is found to have median values around 1000–3000 $m^2\,s^{-1}$ (Fig. 7a). The along-streamline averaged cross-ACC diffusivity shows a minimum of diffusion next to the Antarctic continent, and a northward increase, which reaches a maximum on the equatorward side of the ACC. This maximum is, however, dominated by the few regions of intense mixing. A measure of this inhomogeneity is that the median values of diffusion peaks at approximately 3500 $m^2\,s^{-1}$, substantially lower than the average values (about 4700 $m^2\,s^{-1}$).

5. Data-based scaling estimates

The pattern of weak eddy diffusivity in the core of jets and stronger eddy diffusion outside of the jet is seen repeatedly in geophysical flows (Shuckburgh and Haynes, 2003). Specifically this characteristic has been widely documented in the atmospheric context with the study of the stratospheric vortex, which is characterized by a strong barrier near its core and a surf zone of strong eddy mixing equatorward. The large mixing is thought to be associated with Rossby wave breaking near a critical layer, in which the phase speed of the wave, c, is equal to the mean flow speed, u (e.g. Haynes, 1985; Bower *et al.*, 1985; Marshall *et al.*, 2006; Smith and Marshall, 2009; Shuckburgh *et al.*, 2009; Abernathey *et al.*, 2010). Ferrari and Nikarushin (2010) provide a theory emphasizing the pervasive mixing present in a field of dynamically evolving eddies, which is reduced by mean flow except in the

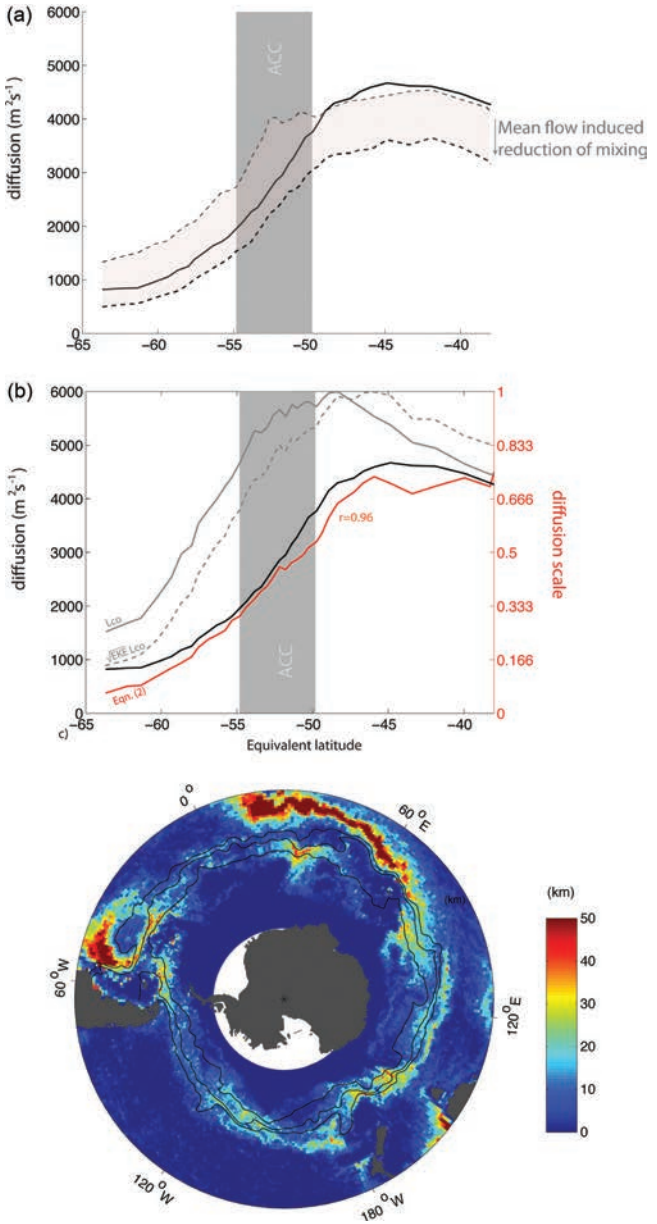

Figure 7. Along-stream averaged diffusion — (a) Along-stream average (plain) and median (dashed black) diffusivity with mean flow turned on. (gray dashed) Median diffusivity with mean flow turned off. (b) (black) Along-stream average diffusivity (same as in panel a) and (red) normalized diffusion scale (Eq. 2); (gray solid) normalized along-stream averaged value of the length scale of coherent eddies L_co; and (gray dashed) normalized along-stream averaged value of $\sqrt{EKE}L_co$. The vertical gray bar represents the mean position of the ACC (Sallée *et al.*, 2008a). (c) Map of the length scale of coherent eddies deduced from altimetry.

vicinity of critical layers. They present a form for the cross-stream surface mixing from SSH assuming a relation between eddy phase speed and mean flow.

To test these ideas we use a simplified scaling and data-based estimates for EKE, eddy length scale, and intrinsic phase speed of eddies:

$$\kappa\alpha\frac{\sqrt{EKE}.L}{1+EKE^{-1}(u-c)^2}, \tag{2}$$

where EKE is the Eddy Kinetic Energy and L the eddy length scale. The form of Eq. 2 has been derived by Ferrari and Nikurashin (2010) from dynamical principles, and is similar to the Taylor (1921) expression for eddy diffusivity: $\kappa = \sqrt{EKE} \cdot \ell$, where $\ell = L/(1 + EKE^{-1}(u - c)^2)$. We estimate the scaling in Eq. 2 with EKE derived from satellite altimetry and the total eddy velocity or intrinsic phase speed (u-c), derived from altimetry by Fu (2009). One fundamental difference with Ferrari and Nikurashin (2010) is that we do not assume the phase speed of eddies to be proportional to the local mean currents, but instead use an observation-based approximation of (u-c). Fu (2009) estimated climatological trajectories or steering of mesoscale eddy variability features (including eddies, meandering jets and waves) from a satellite altimetry analysis of cross-correlation with neighboring time series. Thus, the total eddy velocity represents the the net effect of several processes contributing to eddy displacement. Zero values do not necessarily represent a critical layer for linear waves. We call the stage at which progress is halted 'eddy stagnation."

We use the length scale of coherent eddies (L_{co}) as a measure of the eddy length scale, which we derived from altimetry using the Okubo-Weiss parameter $W = 4((\partial_x u)^2+(\partial_y v)^2)$. This procedure has been used in previous diagnostics of velocity measurements (e.g. Isern-Fontanet *et al.*, 2003; Chelton *et al.*, 2007). Coherent eddies are found by looking for regions in which $W < -8\ 10^{-11}\ \mathrm{s}^{-2}$. Similar to Venaille *et al.* (2011), we define the length scale L of a given structure as an equivalent diameter corresponding to a disk that would have the area of the coherent structure (Fig. 7c).

The overall shape (Eq. 2) of the along-stream averaged cross-stream diffusion predicted by the theory agrees well with that calculated from the particle trajectories (correlation of 0.96, significant at the 99%, Fig. 7b). The scaling predicts a northward increase of mixing from the Antarctic continent to a maximum near 45S. We also examined a simpler scaling $\kappa \propto EKE \cdot T$ with $T = L/(U - c)$ and T bounded by a maximal value, with a resulting similar shape but somewhat poorer agreement. Enhanced mixing on the equatorward side of the jets is largely associated with greater length scale on the northern edge of the ACC, which is not directly related to mean-flow intensity. However, the length scale and EKE do not, by themselves, fully explain the observed distribution, since such a scaling (e.g. $\kappa \propto EKE \cdot L_{co}$) rises too sharply south of the ACC (Fig. 7b).

Although one might consider a critical layer to outcrop on either side of a strong jet, the eddy stagnation regions here bear little resemblance to a coherent outcrop where $u - c \approx 0$. Nevertheless there is some accord with previous studies that have illustrated that

the propagation of geostrophic eddies in the ACC reduces the cross-stream mixing (e.g. Marshall *et al.*, 2006; Shuckburgh *et al.*, 2009; Smith and Marshall, 2009; Ferrari and Nakurashin, 2010). Eddy-mixing is reduced in places where $u \gg c$, and enhanced in places where eddies are arrested, i.e. where $u = c$. The mean flow and topographic steering evidently strongly impact mixing intensity, and our results in Figure 6a show that κ is suppressed so much in the ACC that it is often smaller within the ACC than on its flank, despite the larger EKE.

In order to further test and quantify the impact of mean flow on mixing, we explicitly turned it off and on when advecting particles. Diffusion with mean flow turned off (κ_{off}) presents essentially a similar structure as diffusion with mean flow turned on, but the spots of maximum diffusion are less intense and broader, extending south in the ACC area (Fig. 6b). The mean flow tends to reduce mixing within the ACC (Fig. 6c), although there are locations where the effect is opposite. In agreement with Marshall *et al.* (2006), an averaged reduction of $1000\,m^2\,s^{-1}$, peaking at $1500\,m^2\,s^{-1}$ in the ACC, is observed when mean flow is turned on (Fig. 7a). However, we also find localized areas of large increase in diffusion, up to $1000–2000\,m^2\,s^{-1}$, in the presence of mean flow on the equatorward side of the ACC.

6. Topographic influence on eddy-mixing

Previous studies have noted the influence of topography on lateral mixing intensity in the ACC (Lu and Speer, 2010; Naveira-Garabato *et al.*, 2011; Shuckburgh *et al.*, 2009). These studies have consistently found that topography tends locally to enhance lateral mixing. However, the mechanisms responsible for the enhancement are, so far, not clear. Theoretical work, although often highly idealized, has provided insight into plausible causes. Witter and Chelton (1998) and Thompson (2010) showed in a QG 2-layer model that topography strongly influences the jet regime, either stabilizing the flow and providing a strong barrier to cross-stream mixing, or driving splitting and merging of jets and enhanced mixing. Rhines (2007) showed in lab experiments with a zonal flow on a polar β-plane that a simple spherical-cap mountain produces strong jets and discrete gyres in the wake of the topography and that mixing is conditioned by the wake structures. Therefore we seek next to quantify the role of strong quasi-stationary circulation elements like wakes on the mixing intensity.

Fu (2009) found that eddies and meanders propagate in the Southern Ocean with a velocity of the order of a few kilometers per day, in a predominantly zonal direction, westward outside of the ACC and eastward in the ACC. Directly north of the ACC, the propagation velocity is weaker, except in some particular places where trajectories stagnate and show gyre-like structures (highlighted in red in Fig. 8a). These gyre-like features develop near western boundaries, partially closed bathymetry (e.g. valleys), and in the wake of large bathymetry. In all places where the ACC or the western boundary currents have to flow over large topography, we observe gyre-like structures in the wake of the topography. It is particularly clear in the wake of the Mozambique Rise; the Southwest Indian Ridge; the Southeast Indian Ridge; the Indo-Pacific Ridge; the Campbell Plateau and the Drake

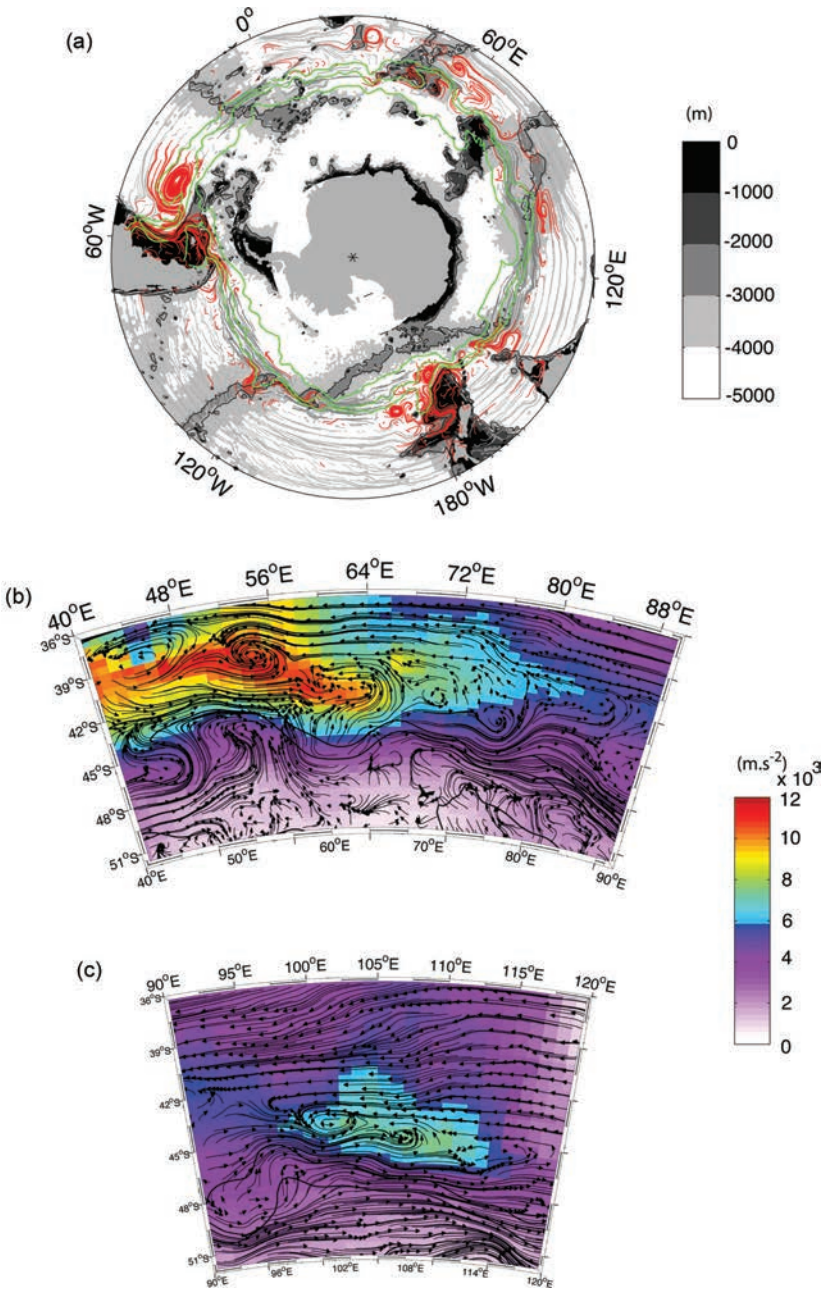

Figure 8. Eddy variability trajectories — (a) Mean eddy variability trajectories from Fu (2009). The trajectories looping in a gyre-like structure are shown in red. Trajectories are superimposed on the Southern Ocean bottom topography. The 3000-m contour is also shown (black). Zoom of eddy variability trajectories in (b) the Crozet–Kerguelen Region and (c) the Southeastern Indian Ridge are superimposed on eddy-mixing intensity. Note that in the Crozet–Kerguelen region, large gyre-like structure develop downstream of Crozet and upstream of Kerguelen.

Passage. Large topographic features such as the Kerguelen Plateau, the Eltanin Fracture Zone or the Mid-Atlantic Ridge steer the flow but are not associated with the gyre-like eddy trajectories. Evidently stronger mean flow sweeps the eddies downstream.

Intensification of mixing is observed in regions of eddy stagnation directly north of the ACC, between the westward propagation of eddy structures farther north of the ACC, and the eastward propagation within the ACC. The increase of mixing near the "stagnation lines" is not clearly related to the critical layer theory. We do not observe a consistent circumpolar mixing intensification; larger mixing develops at the stagnation line only where the line is associated with an enhancement of EKE (Fig. 9). However, EKE itself cannot explain the regional variability of eddy-mixing: there is only a rough agreement at the stagnation line. Our results suggest a departure from the critical layer theory, and are strongly suggestive that the large regional variability of mixing in the Southern Ocean is tightly linked to the combination of the presence of a stagnation band and of large eddy scales, which organize and converge in gyre-like structures downstream of topography.

Mixing magnitude along the stagnation band shows that peaks in the diffusion are associated with the presence of large bathymetric features (Fig. 9b): the Mozambique Rise, the Southwest Indian Ridge and Crozet Island; the eastern Mid-Ocean Ridge in the Indian Ocean; the Macquarie Ridge; the Campbell Plateau; the South American Plateau; and the Mid-Atlantic Ridge. Consistent with some studies, mixing is intensified downstream of topography features (e.g. Rhines, 2007; Witter and Chelton, 1998). For instance, Witter and Chelton (1998) investigated the eddy-mean flow interaction in a idealized case aiming to reproduce the topography of the eastern Indian Ridge. They found that unstable growth rates are largest where the topographic steering forces the jet into regions of reduced ambient PV gradient, increasing eddy energy downstream of topography features. We note, however, that an increase of mixing at the Drake Passage seems to occur at the topographic rise and not downstream.

Although local intensification of eddy mixing is clearly associated with the bottom topography, the overall along-stream magnitude of diffusion seems to be largely shaped by a western versus eastern basin regime for those more northerly portions of the stream. In the three ocean basins, but more clearly in the Indian basin, the diffusion is strongly intensified in the western region. This basin scale pattern is dominated by the highly energetic western boundary current interacting with the ACC on the western edge of each basin (Fig. 1). Diffusion in the western Pacific is less intensified than in the western Atlantic and Indian consistent with the much less energetic western boundary current in the Pacific (see Fig. 1b). The diffusion at the stagnation line, away from the Agulhas Retroflection and the Brazil-Malvinas Confluence (in the region 70°E–70°W) stabilize around a mean value of $3000\,m^2\,s^{-1}$, much lower than in the two very energetic western boundary currents. The lower diffusion is consistent with lower EKE and smaller eddy length scale in the region 70°E–70°W.

As opposed to the relatively high diffusion found along the stagnation line on the northern side of the ACC, the magnitude of cross-stream mixing along the ACC fronts (SAF and

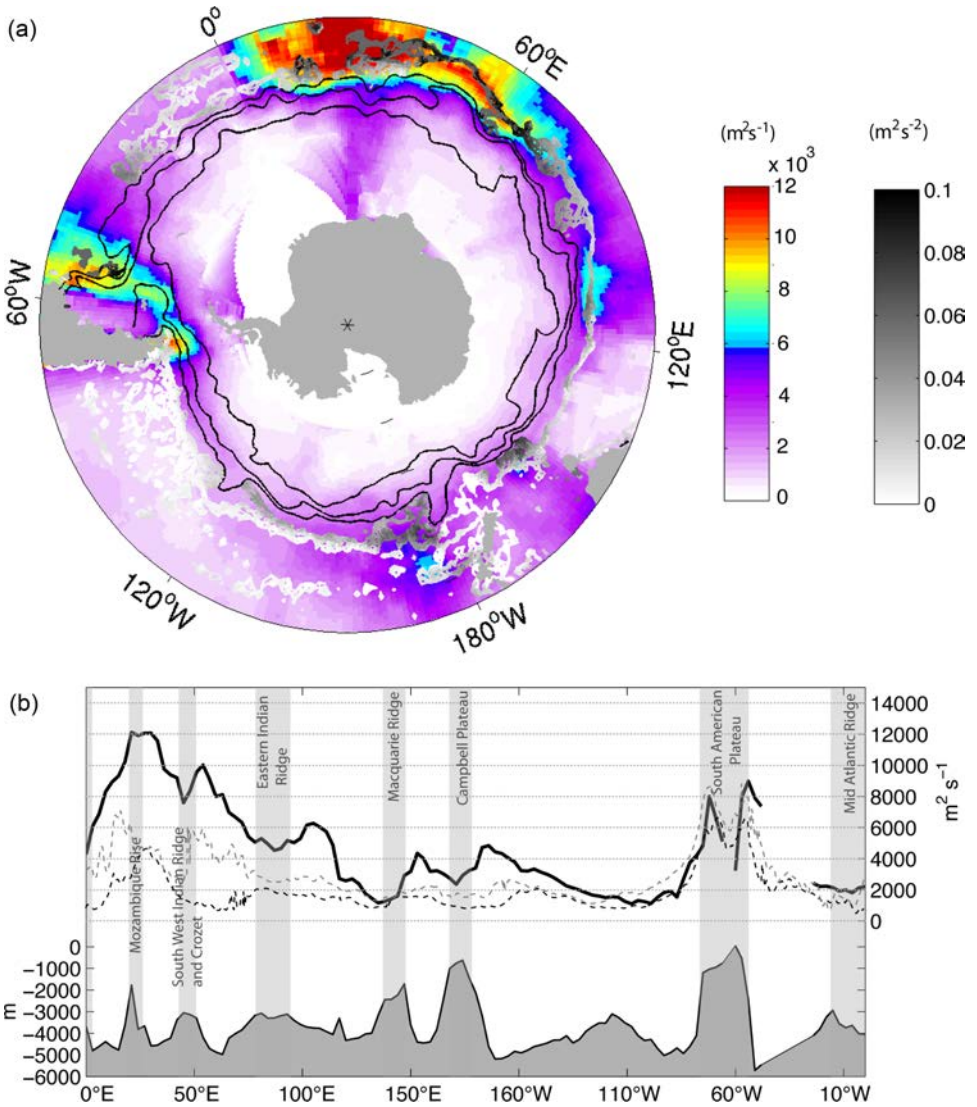

Figure 9. Impact of bathymetry — (a) Eddy stagnation lines superimposed on eddy diffusion coefficient. Stagnation lines are defined as contour lines of eddy displacement velocity in the range $\pm 0.005\,\mathrm{m\,s^{-1}}$, with a step of $0.001\,\mathrm{m\,s^{-1}}$. Stagnation lines are grayscale according to the local value of EKE. (b) Magnitude of eddy-diffusion coefficient along the (black) mean path of the stagnation lines along the circumpolar belt, and corresponding bathymetry depth along the stagnation lines. Magnitude of cross-stream eddy-diffusion along the (dashed black) PF and (dashed gray) SAF are superimposed. Note that the bathymetry below the front position would be different that shown on gray shading, which is the topography along the stagnation lines. Dominant features are however at similar longitudes below the ACC fronts.

PF) is lower (Fig. 9b). As seen above, in the ACC the large jet velocity overcomes the eddy phase speed: meandering dominates and reduces the cross-stream mixing. We find typical values of cross-stream diffusion of 1000–2000 $m^2\ s^{-1}$ in the ACC. There are two very clear increases of mixing in the western Indian Ocean and at Drake Passage, associated with bathymetry. Away from these two extrema, the impact of bathymetry on the cross-stream mixing in the ACC is very clear downstream of the Macquarie Ridge and downstream of the Campbell Plateau. The eastern Indian basin presents an interesting example of topographic control of mixing. In this region, the PF and SAF do not encounter the same topography and this translates into an out of phase regional variability. While the largest topography for the PF is the Kerguelen Plateau at 70°E, the dominant feature for the SAF is the eastern Mid-Indian Ridge at 90°E (Fig. 1). The mixing clearly shows an impact of this on the PF and SAF, with an increase of mixing on the PF downstream of 70°E, followed by an increase of mixing downstream of 90°E on the SAF.

7. Discussion

The 1993–2008 climatological cross-stream mixing intensity of the surface layer of the Southern Ocean has been estimated using satellite altimetry observations. We computed statistics of virtual particle trajectories, numerically advected with surface velocity from satellite. Our choice of dynamic height coordinates has allowed us to distinguish mixing regimes outside and inside jets, as well as to isolate accurately cross-stream dispersion from along-stream dispersion.

The typical values that we find in the ACC (Fig. 9b) are in very good agreement with values from Marshall *et al.* (2006), given the uncertainties in both calculations. The Nakamura (1996) calculation performed by Marshall *et al.* (2006) gives circumpolar integrated values reaching maxima on the northern edge of the ACC of 2000–3000 $m^2\ s^{-1}$, similar to our estimates. In addition, Shuckburgh *et al.* (2009) extended the Marsall *et al.* (2006) results by computing diffusion in local regions in the South Pacific. They found local peaks of diffusion up to 5000 $m^2\ s^{-1}$ in the eastern Pacific basin, while we find diffusion of 4000–6000 in the same region. Indirect support comes from applications of eddy mixing. Values closer to those found in this study have been found to improve the representation of the surface layer circulation, subduction and temperature in coarse resolution models (Danabasoglu and Marshall, 2007; Vivier *et al.*, 2010; Sallée and Rintoul, 2011). Assuming that the eddy phase speed is proportional to mean flow, Ferrari and Nikurashin (2010) obtain diffusivity estimates that are flatter across the ACC and grow on the northern side. Eddy translation estimated from altimetry (Fu *et al.*, 2009) is, however, not correlated with mean flow. Hence we attribute these differences primarily to a more realistic representation of eddy translation in our estimate.

We document how the distribution of cross-stream eddy-mixing is controlled by mean flow, eddy translation or stationarity, and eddy energy, all of which are in turn strongly influenced by bottom topography. We proposed here a simple revised paradigm: (i) the

mean flow shapes the global structure of Southern Ocean mixing, with reduced mixing within the ACC and enhanced mixing north of the ACC at the stagnation line; (ii) the basin-scale asymmetry in eddy kinetic energy, with western boundary intensification, leads to an increase of cross-stream mixing in the western basins; (iii) the flow is destabilized in the wake of topography, causing regional intensification of mixing downstream of large topography, with the largest intensification being associated with eddy convergence at the stagnation line, and weaker intensification within intense jets because of the tendency for the mean-flow to inhibit mixing. The regions of enhanced mixing are found in the wake of large topography and in topographic "valleys" - partially closed f/H contours. While the large-scale pattern of eddy-diffusion is partially explained by the critical theory framework, we also find large regional departures to this theory due to the importance of western boundary currents and topography. The role of topography is consequently appropriately emphasized in the equivalent barotropic models of the ACC (e.g. Krupitsky *et al.*, 1996; LaCasce and Isachsen, 2010).

Although mixing within the ACC is lower than on its equatorward flank, we show that the mixing suppression associated with the ACC jets locally breaks down in the wake of topography. Further observation and modeling (Thompson and Sallée, 2011) shows that cross-frontal particle crossing is strongly localized in the ACC by topographic obstacles, which leads to a rearrangement of the frontal structure and an increase of baroclinicity.

Acknowledgments. KS acknowledges support from NSF OCE-0622670 and NSF OCE 0822075, and dearly appreciated the outbursts of interest in observations that Melvin would come by to express from time to time. SR was supported by the Australian Government's Cooperative Research Centres Programme through the Antarctic Climate and Ecosystems Cooperative Research Centre (ACE-CRC) and by the Australian Climate Change Science Program. The authors thank L. L. Fu for providing the velocity of propagation of the ocean eddy variability.

REFERENCES

Abernathey, R., J. Marshall, M. Mazloff, and E. Shuckburgh. 2010. Enhancement of mesoscale eddy stirring at steering levels in the Southern Ocean. J. Phys. Oceanogr., *40*, 170–184.

Berloff, P. and J. McWilliams. 2002. Material transport in oceanic gyres. Part II: Hierarchy of stochastic models. J. Phys. Oceanogr., *32*, 797–830.

Bower, A. 1991. A simple kinematic mechanism for mixing fluid parcels across a meandering jet. J. Phys. Oceanogr., *21*, 173–180.

Bower, A., H. T. Rossby, and J. Lillibridge. 1985. The Gulf Stream—Barrier or Blender? J. Phys. Oceanogr., *15*, 24–32.

Bracco, A., E. Chassignet, Z. Garraffo, and A. Provenzale. 2003. Lagrangian velocity distributions in a high-resolution numerical simulation of the North Atlantic. J. Atmos. Oceanic Technol., *20*, 1212–1220.

Bracco, A., J. LaCasce, C. Pasquero, and A. Provenzale. 2000a. The velocity distribution of barotropic turbulence. Phys. Fluids. *12*, 2478.

Bracco, A., J. LaCasce, and A. Provenzale. 2000b. Velocity probability density functions for oceanic floats. J. Phys. Oceanogr., *30*, 461–474.

Bryden, H. and R. Heath. 1985. Energentic eddies at the northern edge of the Antarctic Circumpolar Current in the southwest Pacific. Prog. Oceanog., *14*, 65–87.

Chelton, D., M. Sehlax, R. Samelson, and R. de Szoeke. 2007. Global observations of large oceanic eddies. Geophys. Res. Lett., *34*, L15606.

Danabasoglu, G. and J. Marshall. 2007. Effects of vertical variations of thickness diffusivity in an ocean general circulation model. Ocean Model., *18*, 122–141.

Davis, R. 1982. On relating Eulerian and Lagrangian velocity statistics: single particles in homogeneous flows. J. Fluid Mech., *114*, 1–26.

—— 1991. Observing the general circulation with floats. Deep-Sea Res., *38*, S531–S571.

Dong, S., J. Sprintall, and S. Gille. 2006. Location of the Polar Front from AMSR-E satellite sea-surface temperature measurements. J. Phys. Oceanogr., *36*, 2075–2089.

Dritschel, D. and M. McIntyre. 2008. Multiple jets as PV staircases: The Phillips effect and the resilience of eddy-transport barriers. J. Atmos. Sci., *65*, 855–874.

Ducet, N., P. Y. Le Traon, and G. Reverdin. 2000. Global high-resolution mapping of ocean circulation from TOPEX/Poseidon and ERS-1 and -2. J. Geophys. Res., *105*, 19477–19498.

Fahrbach, E., G. Rohardt, M. Schröder, and V. Strass. 1994. Transport and structure of the Weddell Gyre. Annales Geophysicae, *12*, 840–855.

Ferrari, R. and M. Nikurashin. 2010. Suppression of eddy diffusivity across jets in the Southern Ocean. J. Phys. Oceanogr., *40*, 1501–1519.

Fu, L. 2009. Pattern and velocity of propagation of the global ocean eddy variability. J. Geophys. Res., *114*, C11017.

Griesel, A., S. Gille. J. Sprintall, and J. McClean. 2010. Isopycnal diffusivities in the Antarctic Circumpolar Current inferred from Lagrangian floats in an eddying model. J. Geophys. Res., *115*, C06006.

Haynes, P. 1985. Nonlinear instability of a Rossby-wave critical layer. J. Fluid Mech., *161*, 493–511.

Haynes, P., D. Poet, and E. Shuckburgh. 2007. Transport and mixing in kinematic and dynamically-consistent flows. J. Atmos. Sci., *64*, 3640–3651.

Haynes, P. and E. Shuckburgh. 2000. Effective diffusivity as a diagnostic of atmospheric transport. I-Stratosphere. J. Geophys. Res., *105*, 22,777–22,794.

Holloway, G. 1986. Estimation of oceanic eddy transports from satellite altimetry. Nature, *323*, 243–244.

Hughes, C., A. Thompson and C. Wilson. 2010. Identification of jets and mixing barriers from sea level and vorticity measurements using simple statistics. Ocean Model., *32*, 44–57.

Isern-Fontanet, J., E. García-Ladona, and J. Font. 2003. Identification of marine eddies from altimetric maps. J. Atmos. Oceanic Technol., *20*, 772–778.

Joyce, T., W. Zenk, and J. Toole. 1978. Anatomy of the Antarctic Polar Front in the Drake Passage. J Geophys Res. *83*, 6093–6113.

Keffer, T. and G. Holioway. 1988. Estimating Southern Ocean eddy flux of heat and salt from satellite altimetry. Nature, *332*, 624–626.

Klocker. A., R. Ferrari, J. LaCasce, and S. Merrineld. 2011. Reconciling Lagranglan and Eulerian estimates of eddy diffusivities in the Southern Ocean. J Phys. Oceanogr., (submitted).

Krupitsky, A., V. M. Kamenkovich, N. Naik, and M. Cane. 1996. A linear equivalent barotropic model of the Antarctic Circumpolar Current with realistic coastlines and bottom topography. J. Phys. Oceanogr., *26*, 1803–1824.

LaCasce, J. 2000. Floats and f/H. J. Mar. Res., *58*, 61–95.

—— 2008. Lagrangian statistics from oceanic and atmospheric observations. From transport in geophysical flows: Ten years after, *in* Transport and Mixing in Geophysical Flows. J. Weiss and A. Provenzak, eds., 262pp.

LaCasce, J. and P. Isachsen. 2010. The linear models of the ACC. Prog. Oceanogr., *84*, 139–157.

LaCasce, J. and K. Speer. 1999. Lagrangian statistics in unforced barotropic flows. J. Mar. Res., *57*, 245–274.

LeTraon, P. Y., F. Nadal and N. Ducet. 1998. An improved mapping method of multisatellite altimeter data. J. Atmos. Tech, *15*, 522–534.

Lu, J, and K. Speer. 2010. Topography, jets, and ecidy mixing in the Southern Ocean. J. Mar. Res., *68*, 479–502.

Marshall, J., E. Shuckburgh, H. Jones, and C. Hill. 2006. Estimates and implications of surface eddy diffusivity in the Southern Ocean derived from tracer transport. J. Phys. Oceanogr., *36*, 1806–1821.

Marshall, J. and G. Shutts. 1981. A note on rotational and divergent eddy fluxes. J. Phys. Oceanogr., *11*, 1677–1680.

Maurizi, A., A. Griffa, P. Poulain, and F. Tampieri. 2004. Lagrangian turbulence in the Adriatic Sea as computed from drifter data: effects of inhomogeneity and nonstationarity. J. Geophys. Res. *109*, C04010.

Moore, J. K., M. R. Abbott, and J. G. Richman. 1999. Location and dynamics of the Antarctic Polar Front from satellite sea surface temperature data. J. Geophys. Res., *104*, 3059–3073.

Morrow, R., A. Brut, and A. Chaigneau. 2003. Seasonal and interannual variations of the upper ocean energetics between Tasmania and Antarctica. Deep-Sea Res., *50*, 339–356.

Nakamura, N. 1996. Two-dimensional mixing, edge formation, and permeability diagnosed in an area coordinate. J. Atmos. Sci., *53*, 1524–1537.

Naveira-Garabato, A., R. Ferrari, and K. Polzin. 2011. Eddy-induce mixing in the Southern Ocean. J. Geophys. Res., *116*, C09019.

Nowlin, W. J., S. Worley, and T. Whitworth III. 1985. Methods for making point estimates of eddy heat flux as applied to the Antarctic Circumpolar Current. J. Geophys. Res., *90*, 3305–3324.

O'Dwyer, J., R. Williams, J. LaCasce, and K. Speer. 2000. Does the potential vorticity distribution constrain the spreading of floats in the North Atlantic? J. Phys. Oceanogr., *30*, 721–732.

Phillips, H. and S. Rintoul. 2000. Eddy variability and energetics from direct current measurements in the Antarctic Circumpolar Current south of Australia. J. Phys. Oceanogr., *30*, 3050–3076.

Pratt, L., M. Lozier, and N. Beliakova. 1995. Parcel trajectories in quasigeostrophic jets: Neutral modes. J. Phys. Oceanogr., *25*, 1451–1466.

Rhines. P. 2007. Jets and orography: Idealized experiments with tip jets and lighthill blocking J. Atmos. Sci., *64*, 3627–3639.

Rio, M., P. Schaeffer, F. Hernandez, and J. Lemoine. 2005. The estimation of the ocean mean dynamic topography trough the combination of altimetric data, *in-situ* measurements and GRACE geoid: from global to regional studies. Proceedings of the GOCINA international workshop, Luxembourg.

Rupolo, V. 2007. A Lagrangian-based approach for determining trajectories taxonomy and turbulence regimes. J. Phys. Oceanogr., *37*, 1584–1609.

Sallée, J. B. and S. Rintoul. 2011. Parameterization of eddy-induced subduction in the Southern Ocean surface-layer. Ocean Model., *39*, 146–153.

Sallée, J., K. Speer, and R. Morrow. 2008a. Response of the Antarctic Circumpolar Current to atmospheric variability. J. Climate, 21, 3020–3039.

Sallée, J., K. Speer, R. Morrow, and R. Lumpkin. 2008b. An estimate of Lagrangian eddy statistics and diffusion in the mixed layer of the Southern Ocean. J. Mar. Res., *66*, 441–463.

Sallée, J., R. Morrow, and K. Speer. 2008c. Eddy heat diffusion and Subantarctic Mode Water. Geophys. Res. Lett., *35*, L05607.

Sallée, J., K. Speer, S. Rintoul, and S. Wijffels. 2010. Southern Ocean thermocline ventilation. J. Phys. Oceanogr., *40*, 509–529.

Sallée, J., N. Wienders, K. Speer, and R. Morrow. 2006. Formation of subantarctic mode water in the southeastern Indian Ocean. Ocean Dyn., *56*, 525–542.

Schröder, M. and E. Fahrbach. 1999. On the structure and the transport of the eastern Weddell Gyre. Deep-Sea Res. II, *46*, 501–527.

Shuckburgh, E. F. and P. Haynes. 2003. Diagnosing transport and mixing using a tracer-based coordinate system. Phys. Fluids, *15*, 3342–3357.

Shuckburgh, E., H. Jones, J. Marshall, and C. Hill. 2009. Understanding the regional variability of eddy diffusivity in the Pacific sector of the Southern Ocean. J. Phys. Oceanogr., *39*, 2011–2023.

Sinha, B. and K. J. Richards. 1999. Jet structure and scaling in Southern Ocean models. J. Phys. Oceanogr., *29*, 1143–1155.

Smith, K. and J. Marshall. 2009. Evidence for enhanced eddy mixing at middepth in the Southern Ocean. J. Phys. Oceanogr., *39*, 50–69.

Sokolov, S. and S. Rintoul. 2007. Multiple jets of the Antarctic Circumpolar Current south of Australia. J. Phys. Oceanogr., *37*, 1394–1412.

—— 2009a. Circumpolar structure and distribution of the Antarctic Circumpolar Current fronts: 1. Mean circumpolar paths. J. Geophys. Res., *114*, C11018.

—— 2009b. Circumpolar structure and distribution of the Antarctic Circumpolar Current fronts: 2. Variability and relationship to sea surface height. J. Geophys. Res., *114*, C11019.

—— 2002. Structure of Southern Ocean, fronts at 140E. J. Mar. Syst. *37*, 151–184.

Stammer, D. 1998. On eddy characteristics, eddy transports, and mean flow properties. J. Phys. Oceanogr., *28*, 727–739.

Taylor, G. 1921. Diffusion by continuous movements. P. Lond. Math. Soc., *20*, 196–212.

Thompson, A. 2010. Jet formation and evolution in baroclinic turbulence with simple topography. J. Phys. Oceanogr., *40*, 257–278.

Thompson, A. and J. Sallée. 2011. Jets and topography: jet transitions and impacts on transport. J. Phys. Oceanogr., (submitted).

Traon, P. L., F. Nadal, and N. Ducet. 1998. An improved mapping method of multisatellite altimeter data. J. Atmos. Oceanic Technol., *15*, 522–534.

Venaille, A., G. K. Vallis, and K. S. Smith. 2011. Baroclinic turbulence in the ocean: analysis with primitive equation and quasigeostrophic simulations. J. Phys. Oceanogr., (submitted), *41*, 1605–1623.

Veneziani, M., A. Griffa, Z. Garraffo, and E. Chassignet. 2005. Lagrangian spin parameter and coherent structures from trajectories released in a high-resolution ocean model. J. Mar. Res., *63*, 753–788.

Veneziani, M., A. Griffa, A. M. Reynolds, and A. J. Mariano. 2004. Oceanic turbulence and stochastic models from subsurface Lagrangian data for the northwest Atlantic Ocean. J. Phys. Oceanogr., *34*, 1884–1906.

Vivier, F., D. Iudicone, F. Busdraghi, and Y. Park. 2010. Dynamics of sea-surface temperature anomalies in the Southern Ocean diagnosed from a 2D mixed-layer model. Climate Dyn. *34*, 153–184.

Waugh, D. and E. Abraham. 2008. Stirring in the global surface ocean. Geophys. Res. Lett., L20605.

Waugh, D., L. Polvani, and R. Plumb. 1994. Nonlinear, barotropic response to a localized topographic forcing: Formation of a "tropical surf zone" and its effect on interhemispheric propagation. J. Atmos. Sci. *51*, 1401–1416.

Witter, D. L. and D. B. Chelton. 1998. Eddy-mean plow interaction in Zonal oceanic jet flow along zonal ridge topography. J. Phys. Oeeanogr., *28*, 2019–2039.

Zhurbas, V. and I. S. Oh. 2004. Drifter-derived maps of lateral diffiisivity in the Pacific and Atlantic Oceans in relation to surface circulation patterns. J. Geophys. Res., *109*, 1–10.

Received: *12 May, 2011*; revised: *21 December, 2011*.